UNIVERSITY *of* York

This is a repository copy of *Influence of Antipodally Coupled Iodine and Carbon Atoms on the Cage Structure of 9,12-I2-closo-1,2-C2B10H10:An Electron Diffraction and Computational Study*.

White Rose Research Online URL for this paper:
https://eprints.whiterose.ac.uk/93796/

Version: Accepted Version

Article:

White Rose
university consortium
Universities of Leeds, Sheffield & York

eprints@whiterose.ac.uk
https://eprints.whiterose.ac.uk/

The influence of antipodally coupled iodine and carbon atoms on the cage structure of 9,12-I$_2$-*closo*-1,2-C$_2$B$_{10}$H$_{10}$: an electron diffraction and computational study

Yury V. Vishnevskiy,*[†] Denis S. Tikhonov,[†,‡] Christian G. Reuter,[†] Norbert W. Mitzel,*[†] Drahomír Hnyk,*[§] Josef Holub,[§] Derek A. Wann,*[∥] Paul D. Lane,[∥,⊥] Raphael J. F. Berger,[$] and Stuart A. Hayes[†]

[†] Universität Bielefeld, Universitätsstraße 25, D-33615 Bielefeld, Germany.

[‡] M. V. Lomonosov Moscow State University, Department of Physical Chemistry, GSP-1, 1-3 Leninskiye Gory, 119991, Moscow, Russian Federation.

[§] Institute of Inorganic Chemistry of the ASCR, v.v.i, CZ-250 68 Husinec-Řež, Czech Republic.

[∥] Department of Chemistry, University of York, Heslington, York, U.K. YO10 5DD.

[⊥] Current address: School of Engineering and Physical Sciences, Heriot-Watt University, Edinburgh, U.K. EH14 4AS.

[$] Materialchemie, Paris-Lodron Universität Salzburg, Hellbrunner Str. 34, A-5020 Salzburg, Austria.

■ AUTHOR INFORMATION

Corresponding Author

* E-mail: yury.vishnevskiy@uni-bielefeld.de (Y.V.V.); hnyk@iic.cas.cz (D.H.); derek.wann@york.ac.uk (D.A.W.); norbert.mitzel@uni-bielefeld.de (N.W.M.).

ABSTRACT:

Due to the comparable electron-scattering abilities of carbon and boron, the electron-diffraction structure of the C_{2v}-symmetric molecule *closo*-1,2-$C_2B_{10}H_{12}$ (**1**), one of the building blocks of boron cluster chemistry, is not as accurate as it could be. On that basis, we have prepared the known diiodo derivative of (**1**), 9,12-I_2-*closo*-1,2-$C_2B_{10}H_{10}$ (**2**), which has the same point-group symmetry as **1**, but where the presence of iodine atoms, with their much greater ability to scatter electrons, ensures much better structural characterization of the C_2B_{10} icosahedral core. Furthermore, the influence on the C_2B_{10} geometry in **2** of the antipodally positioned iodine substituents with respect to both carbon atoms has been examined using the concerted application of gas electron diffraction and quantum-chemical calculations at the MP2 and DFT levels. The experimental and computed molecular geometries are in good overall agreement. Molecular dynamics simulations used to obtain vibrational parameters, which are needed for analyzing the electron diffraction data, have been performed for the first time for this class of compound. According to DFT calculations at the ZORA-SO/BP86 level, the ^{11}B chemical shifts of the boron atoms to which the iodine substituents are bonded are dominated by spin-orbit coupling. Magnetically-induced currents within **2** have been calculated and compared to those for $[B_{12}H_{12}]^{2-}$, the latter adopting a regular icosahedral structure with I_h point-group symmetry. Similar total current strengths are found but with a certain anisotropy, suggesting that spherical aromaticity is present; electron delocalization in the plane of the hetero atoms in **2** is slightly hindered compared to that for $[B_{12}H_{12}]^{2-}$, presumably caused by the departure from ideal icosahedral symmetry.

■ INTRODUCTION

Polyhedral borane and carbaborane clusters are notable for the presence of delocalized electron-deficient bonding.[1] As there are too few valence electrons for bonding to be described exclusively in terms of 2-center-2-electron (2c-2e) bonds, one characteristic of electron-deficient structures is the aggregation of atoms to form 3-center-2-electron (3c-2e) bonds, which typically result in the formation of trigonal faces and hypercoordination.

The three-dimensional deltahedral shapes typical of boron and carbaborane clusters are described, with reference to their formal electron counts,[2] by the terms *closo*, *nido*, *arachno*, and *hypho*. The *closo* clusters are of particular current interest as they possess especially high thermal and chemical stability. The number of vertices, n, can range from 5 to 12; *closo* clusters with higher values of n usually contain one or more metal atoms.[3]

Deltahedral *closo* boranes have the formula $B_nH_n^{2-}$, with the 12-vertex icosahedral cluster, $B_{12}H_{12}^{2-}$ (point-group symmetry I_h), being the most common and most stable of the series.[3b] The replacement of one or more boron atoms at a vertex by atoms of other elements results in the formation of *closo* heteroboranes. Since a CH unit is isoelectronic with a BH^- moiety the simplest *closo*-carbaborane is the monoanionic *closo*-$[CB_{11}H_{12}^-]$;[4] it contains a five-coordinate carbon atom, sometimes referred to as hypercarbon.[5] Replacing two BH^- groups by two CH moieties yields the neutral dicarbaboranes $C_2B_{10}H_{12}$ in a variety of three isomers differing in the relative positions of the hypercarbon atoms. The 1,2-isomer (the so-called *o*-carbaborane with C_{2v} symmetry; see Figure 1 for the molecular structure) is the least stable isomer and the one with the largest dipole moment.[6] Consequently, terminal hydrogens bonded to the atoms B(9) and B(12) [antipodally coupled with C(1,2)][7] are quite hydridic and can be easily replaced by, for example, halogens atoms or SH groups.[8]

Figure 1. The geometric structure of *closo*-1,2-$C_2B_{10}H_{12}$ (**1**) with heavy-atom numbering.
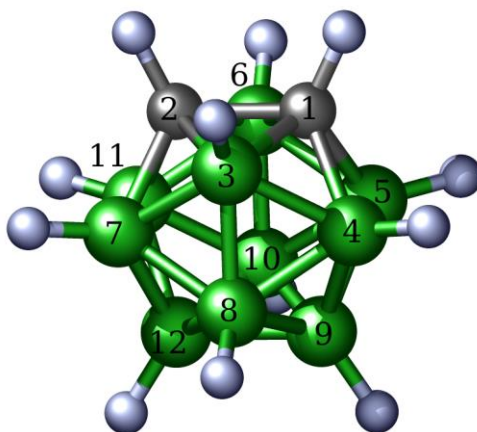
The molecule *closo*-1,2-$C_2B_{10}H_{12}$ (**1**) is quite spherical and, therefore, due to orientation disorder in the crystal, there is no solid-state structure available in the Cambridge Structural Database. However, this material is relatively easy to evaporate, which is essential for applying both gas electron diffraction (GED) and microwave spectroscopy (MW) – two key structural methods for gas-phase studies. Indeed, both gas-phase structures are known and agree well with one another.[9] In order to determine the structure of the carbaborane core accurately, the GED analysis[9b] required the application of many flexible restraints to parameters using the SARACEN method.[10] It is known that the accuracy increases even further if the terminal hydrogen atoms are replaced by heavier elements since their electron scattering ability is larger than that of hydrogen.

It has been demonstrated quite recently that the presence of two SH groups bonded to B(9) and B(12) is quite helpful for accurate structural determination of the carbaborane core by GED.[11] In order to gain a deeper insight into the structure of the 9,12-substituted carbaborane moiety, we have undertaken the determination of the GED structure of 9,12-I_2-*closo*-1,2-$C_2B_{10}H_{10}$ (**2**). To this end a number of diffraction refinement methods have been undertaken as well as different ways of computing amplitudes of vibration and distance corrections.

Quantum-chemical calculations of various variables using different model chemistries were also carried out for comparison with the experimental results.

■ EXPERIMENTAL SECTION

Synthesis. A sample of **2** was prepared according to procedure reported in the literature,[12] where the crystalline structure is also reported. **2** was isolated from the mixture that also contained the 8,9-diodo derivative of **2** by means of column chromatography.

NMR Measurements. ^{11}B NMR spectroscopic measurements were performed at 11.75 T using a Varian XL-500 instrument in CD_3CN, using also the $^{11}B\{^1H\}$-$^{11}B\{^1H\}$ COSY 2D approach.

Computational Details. Geometry optimizations and second derivative analyses of **2** were performed assuming C_{2v} point-group symmetry using the Gaussian09 suite of programs.[13] The structure was optimized at the frozen-core MP2 [MP2(fc)] level, using two different basis sets. Initially, the 6-31G* basis set[14] was used for H, B, and C, while the quasirelativistic energy-consistent pseudopotential (ECP)[15] with DZP basis set was used for I. Later optimizations used the SDB-cc-pVTZ basis set, *i.e.* with Stuttgart-Dresden-Bonn relativistic effective core potentials. Both optimizations of **2** were found to represent minima on the respective potential hypersurfaces.

Amplitudes of Vibration and Distance Corrections. In order to obtain vibrational amplitudes and distance corrections additional structure optimizations were performed at B3LYP/SDB-cc-pVTZ and PBE0/def2-SV(P) computational levels followed by Hessian and cubic force-field computations. Again, no imaginary frequencies were found in these harmonic vibrations analyses.

Vibrational amplitudes and ($r_e - r_a$) distance corrections were computed using the programs SHRINK[16] and ELDIFF[17] with the B3LYP/SDB-cc-pVTZ and PBE0/def2-SV(P) force fields.

Values obtained from PBE0/def2-SV(P) calculations were used for comparison with values computed from MD simulations.

Molecular Dynamics (MD) Simulations. For MD simulations the GAMESS US[18,19] quantum-chemical package was used. Gradients were calculated at the PBE0/def2-SV(P) approximation level. The simulations were carried out at the estimated temperature of the GED experiment (481 K), using a canonical (NVT) ensemble modeled using the Nosé-Hoover thermostat[20] and the velocity rescaling with the allowed temperature range defined as the three times temperature fluctuation of the ideal gas using formula $\Delta T = 3T\sqrt{(2 / N_f)}$, where T is the simulation temperature, and N_f is the number of degrees of freedom, which was 72 in the present case. The trajectory length was 3.3 ps with a time step of 0.2 fs. The first 0.2 ps were skipped during the parameters calculation to account for the equilibration phase. The calculation of the MD trajectory was started from equilibrium geometry. Vibrational amplitudes and distance corrections were obtained from MD trajectories using our own program Qassandra which was previously tested to give same results as the MDVibCor program.[21,22] The main reason of using the new program was its ability to account for quantum effects and thus allowing calculations of vibrational amplitudes and corrections with higher accuracy.

NMR Calculations. Calculations of shielding tensors with gauge-including atomic orbitals (GIAO) were performed at the MP2 level using IGLO-II all-electron basis sets[23] for H, B, and C, and the same ECP and DZP basis sets for I as were used for the earlier optimizations. Additional NMR calculations were performed using the same geometries as in the quasi-relativistic GIAO-MP2 computations with the Amsterdam Density Functional (ADF) code[24] employing the BP86 functional. The two-component relativistic zeroth-order regular approximation (ZORA) method[25] including scalar and spin-orbit (SO)[26] corrections was employed for these computations; the all-electron triple-zeta basis set plus one polarization function (denoted TZP; from the ADF library) was used for all atoms. Magnetic shieldings

6

were converted into relative [11]B chemical shifts using ^{11}B NMR of B_2H_6 as the primary reference.[27]

Magnetically-Induced Ring Current Calculations. All calculations have been performed using Turbomole (version 6.2). The geometry was optimized at RI-DFT(BP86)/TZVP level of theory with default settings. The perturbed densities were calculated with Turbomole's mpshift module. GIMIC[28] was used for the calculation of the magnetically-induced current field vectors.

Gas Electron Diffraction. The electron diffraction patterns were recorded on the recently improved Balzers Eldigraph KDG2 gas electron diffractometer[29] at Bielefeld University. Data were collected at two different nozzle-to-detector distances, namely 250.0 and 500.0 mm, with the samples heated to 479 and 482 K, respectively. The full experimental conditions are presented in Table S1 in Supporting Information. The electron diffraction patterns were measured on Fuji BAS IP MP 2025 imaging plates, which were scanned using a calibrated Fuji BAS 1800II scanner. The intensity curves (Tables S2 and S3, Figures S1–S5 in SI) were obtained by applying the method described in detail elsewhere.[30] Electron wavelengths were refined[31] using diffraction patterns of CCl_4, recorded along with the substances under investigation.


■ **RESULTS AND DISCUSSION**

Amplitudes of Vibrations and Distance Corrections. Amplitudes of vibration and distance corrections have been calculated using SHRINK[16] and ELDIFF[17] programs, both of which use similar theoretical and numerical bases and require harmonic or cubic force fields for an equilibrium geometry to be calculated. The equilibrium geometry and force fields were calculated using the PBE0/def2-SV(P) quantum-chemical method. An alternative MD method has also been used for obtaining amplitudes of vibration and distance corrections. This

method is described in more detail in Supporting Information with comparisons of results in Table S4.

Gas Electron Diffraction Structural Analysis. In general, GED experiments allow the direct observation of thermally averaged structure parameters (r_a). It is, however, possible to estimate equilibrium geometries (r_e) from these measured values; these are comparable to those obtained from quantum chemistry.[32] To do this requires knowledge of anharmonic force fields to calculate the required corrections.[16,17] Another way to calculate such corrections is to use molecular dynamics (MD) simulations.[21,22] Both approaches are applicable to the calculation of vibrational amplitudes, which are needed in GED structural analyses. Molecule **2** is a good candidate for comparison of vibrational parameters calculated from MD trajectories with those computed using standard methods.[16,17] This molecule is relatively large but still allows calculation of a cubic force fields using DFT theory with reasonable basis sets.

Figure 2. The molecular geometry of 9,12-I_2-*closo*-1,2-$C_2B_{10}H_{10}$ (**2**) showing carbaborane core numbering.
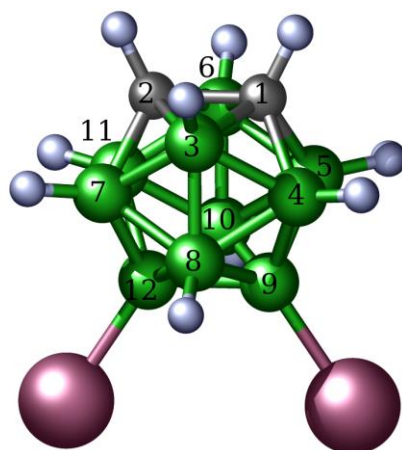
Least-squares structure refinements were carried out using the UNEX program.[33] Two averaged intensity curves from long and short nozzle-to-detector distances were used for the analysis (see Tables S2 and S3). Averaging was carried out using three independent experimental curves for each nozzle-to-plate distance. The background was eliminated in a

8

multiplicative model using cubic splines. The molecule was assumed to have C_{2v} symmetry in all models. Amplitudes were optimized in three groups using scaling multipliers which kept the ratios of the values in one group the same as obtained from the theoretical model.

Z-matrix Model. To refine the structure of **2** its molecular geometry was initially defined using a Z-matrix, whose parameters are listed in Table S5 of the SI. This model (**2a**) was constructed using the MP2/SDB-cc-pVTZ equilibrium geometry and B3LYP/SDB-cc-pVTZ force fields processed with the SHRINK program to obtain vibrational amplitudes and distance corrections (for the calculated data, see Tables S6 and S7 in SI). In general, the main disadvantage of this model was related to the fact that the geometry definition in terms of the Z-matrix made it impossible to apply constraints to geometrically dependent parameters. As a consequence, some of the refined B–B bond lengths were significantly longer than expected. The average bond length for dependent B–B bonds (those that were not refining) was 0.06 Å longer than for the independent (refining) ones, a trend that was not observed in our quantum-chemical calculations. Results for model **2a** are given in Table 1 and in Table S8 in SI.

Table 1. Experimental (gas-phase and crystalline) and calculated geometrical parameters for 9,12-I$_2$-*closo*-1,2-C$_2$B$_{10}$H$_{10}$, **2**.[a,b]

Parameter/Model	GED-**2a** $r_e, \angle_e$	GED-**2e** $r_e, \angle_e$	GED-**2b** $r_e, \angle_e$	r_g	MP2/SDB-cc-pVTZ	XRD[12c]
rC–C	1.623(5)	1.619(34)	1.621(18)	1.637(18)	1.622	1.626(15)
rB–C[c]	1.706(5)	1.690(21)	1.699(10)	1.715(10)	1.705	1.708(16)
rB–B[c]	1.774(15)	1.784(24)	1.778(12)	1.793(12)	1.782	1.781(16)
rB–I	2.141(9)	2.129(15)	2.139(8)	2.148(8)	2.150	2.178(11)
rC–H[c]	1.082(11)	1.098(24)	1.088(12)	1.108(12)	1.080	1.000
rB–H[c]	1.182(11)	1.182(30)	1.183(13)	1.205(13)	1.179	1.120
$\angle$(C–C–B)[d]	61.80(1)	61.7(6)	61.8(3)		61.8	61.7(6)
$\angle$(C–C–B)[e]	111.5(2)	112.0(8)	111.7(4)		111.8	111.8(9)
$\angle$(C–B–C)	56.40(1)	56.6(12)	56.4(6)		56.4	56.5(6)
$\angle$(C–B–B)[d]	58.3(2)	58.2(9)	58.4(4)		58.4	58.5(6)
$\angle$(C–B–B)[e]	103.1(4)	103.6(12)	103.9(6)		103.9	104.0(9)
$\angle$(B–C–B)[d]	63.4(5)	63. 7(10)	63.2(5)		63.1	63.0(6)
$\angle$(B–C–B)[e]	116.9(2)	117.0(10)	116.2(6)		116.0	115.7(9)
$\angle$(B–B–B)[d]	60.0(6)	60.0(9)	60.0(4)		60.0	60.0(15)
$\angle$(B–B–B)[e]	108.3(6)	108.0(12)	108.0(6)		108.0	108.1(8)
$\angle$(B–B–I)[c]	121.8(7)	122.0(9)	121.8(4)		121.6	121.4(6)
$\angle$(C–C–H)[c]	116.2	115.8(15)	116.0(7)		116.2	120.8
$\angle$(B–B–H)[c]	123.6(3)	123.4(16)	123.6(7)		123.6	122.0
$\angle$(C–B–H)[c]	118.1	119.0(15)	118.2(7)		118.1	125.3
R_{str}[f], %	5.64	7.40	6.03		11.86[g]	3.4

[a] Distances are in Å, angles are in degrees. [b] Numbers in parentheses are threefold standard deviations. For average parameters the error limits were calculated from standard deviations of individual parameters as $3\sigma_{av} = 3 \cdot \sqrt{\sum_{i=1}^{N} \sigma_i^2 / N}$, where σ_i is the standard deviation of the *i*th parameter, and *N* is the number of averaged parameters. [c] Average of all geometrical parameters of this type. [d] Average of the narrow angles of this type. [e] Average of the wide angles of this type. [f] Total structural *R* factor. [g] *R* factor obtained only by scaling intensity curves to corresponding geometry with vibrational amplitudes and distances correction from B3LYP/SDB-cc-pVTZ force-field calculations.

Cartesian-Coordinate Models. Due to the problems encountered with the Z-matrix model (**2a**), we arrived at a decision to construct a new model (**2b**) with its geometry based on Cartesian coordinates (see Table S9 in SI). These coordinates were refined as parameters of the model with their theoretical values at the MP2/SDB-cc-pVTZ level used additionally for regularization (Table S6 in SI). The latter was needed in order to ensure a stable least-squares refinement and obtain physically meaningful results in the structural analysis. In this case the functional for minimization Q was defined as:

$$Q = \sum_i \left[sM(s)_i^{\text{exp}} - sM(s)_i^{\text{model}} \right]^2 + \alpha \sum_j \left(x_j^0 - x_j \right)^2 ,$$

where the regularization parameter α determines the relative amount of theoretical information used as flexible restraint in the least-squares procedure. The vibrational amplitudes and corrections were the same as in the model **2a**.

To investigate the dependence of the results on the regularization parameter several optimizations were performed with different values of α varying from 0.001 to 10000. To determine the final value of α, three heuristic criteria were tested. The first one was the L-curve criterion.[34] This method did not give reliable results because of the instability of the functional in the vicinity of the desired point. Therefore, no clear bending of the curve could be seen (see Figure S6 in SI). The second one was the Maximum Product Criterion (MPC).[35] Although this criterion was developed for the other type of inverse problem, we applied it in our research obtaining value $\alpha = 40$. Finally, the last one was a criterion in which the ratio of the optimized GED part of the total functional to the regularization part should be equal to the regularization parameter α. It can be thought as a simplified variant of a heuristic criterion suggested earlier.[36] This criterion gave a value of $\alpha = 8$, which was chosen as the final value (see Table 1 and Table S10 in SI), since it gave the most reasonable results and was closer to the area were the L-curve was expected to change its direction. In order to check the applicability of vibrational amplitudes and distance corrections obtained from MD

11

simulations three additional models were constructed. All of them used the last criterion for the regularization parameter choice. For comparison model (**2c**) was constructed based on PBE0/def2-SV(P) force fields processed with the SHRINK program. The regularization parameter for this model was found to be 7. The refined in this model molecular structure (see Table S11 in SI) was very similar to that in model **2b**. Another model (**2d**) employed the PBE0/def2-SV(P) approximation for MD simulations, with the results processed using the in-house program Qassandra applying the previously published method[21,22] (see Table S12 in SI).

Finally, a model (**2e**) was created using vibrational amplitudes and corrections calculated on the basis of PBE0/def2-SV(P) MD simulations corrected to account for quantum effects (see Table S13 in SI). The corresponding theoretical and computational details are given in SI. The results obtained for models **2a**, **2b** and **2e** are listed in Table 1, where the refined parameters are seen to generally agree within the experimental errors. This indicates that it is possible to use vibrational parameters calculated on the basis of MD simulations with quantum corrections. For the refinement based on model **2e** the B–I bonds were slightly shorter, which was directly related to variations in the $(r_e - r_a)$ distance corrections calculated using force fields (Table S14 in SI) and MD simulations (Tables S15 and S16 in SI). In summary, model **2b** was considered to be the optimal and was therefore accepted to be the final one. Inspection of the final radial distribution curve (RDC; see Figure 3) reveals that the carbaborane core is precisely determined since there are quite discernible peaks associated with B⋯I, C⋯I and I⋯I terms. The corresponding RDCs for models **2a**, **c**, **d** and **e** are shown in Figures S7–S10, while the molecular scattering curves for models **2a**-**e** are given in Figures S11–S15. Correlation matrices for refinements of each of models **2a**-**e** are shown in Tables S17–S21.

Figure 3. Model (line) and experimental (dots) radial distribution functions for **2** obtained in model **2b**, difference curve is shown below.
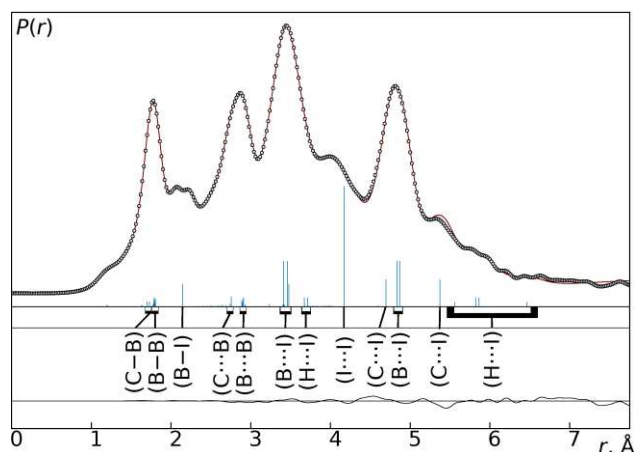
The geometry of the carbaborane core in **2** is similar to that in **1**[9] and in its 9,12-(SH)$_2$ analogue.[11] There is also generally good agreement between the GED and XRD[12c] structures (see Table 1), but such a comparison must be taken with caution because of the entirely different physical meaning of interatomic separations determined by these two diffraction methods. The structural findings for **2** support a general observation that *exo* substituents bonded to cluster atoms interact with them only marginally causing very little structural change.

NMR Results. ZORA computations were performed for the structures yielded by each of refinement models **2a-e**. The result that best matched the experimental NMR chemical shifts was for **2b**, further demonstrating that model **2b** is the most reliable one.

Inspection of Table 4 reveals that there is relatively good agreement between the GIAO-MP2/II-computed and experimental ^{11}B chemical shifts for **2** apart from those boron atoms that are bonded to iodine substituents. Calculations using all three geometries (two calculated ones and the GED geometry) perform almost equally in terms of this agreement. Since inclusion of scalar relativistic effects by pseudopotentials in the GIAO calculations (*i.e.* without spin-orbit effects) does not solve the problem, these discrepancies indicate the need for an appropriate level of theory that takes into account the effect of relativistic spin-orbit

(SO) coupling[37] on the chemical shifts. Such effects are known to overcompensate for the trends caused by decreasing electronegativity for the heavier halogen substituents.[38] Indeed, employing the two-component relativistic zeroth-order regular approximation (ZORA) method within the ADF code, in order to account for the SO corrections to the ^{11}B shifts in the B(9) and B(12) positions for **2**, improves the fit between theory and experiment for these atoms considerably (SO contributions amounts to *ca.* 21 ppm for all three geometries considered), as Table 2 also shows. GIAO results for B(3,6) and B(4,5,7,11) are superior to those provided by ZORA computations. The influence of SO coupling on the chemical shifts can also be visualized by the relativistic contribution to the magnetically induced current density (*vide infra*).

Table 2 ^{11}B chemical shifts for **2** with respect to BF$_3$·OEt$_2$.

	B(3,6)	B(4,5,7,11)	B(8,10)	B(9,12)
ZORA^a//MP2/SDB^b	−20.1	−17.6	−8.0	−13.8
ZORA^a//MP2/DZP^c	−20.4	−17.7	−8.4	−13.9
ZORA^a//GED(**2b**)^d	−20.5	−17.8	−8.0	−13.5
GIAO^e//MP2/SDB^b	−15.6	−12.0	−3.8	8.2
GIAO^e//MP2/DZP^c	−15.7	−12.0	−4.2	8.6
GIAO^b//GED(**2b**)^d	−15.9	−12.2	−3.7	8.5
Exp.	−14.4	−13.0	−6.5	−15.2
Exp.^{f}	−14.5	−13.2	−6.0	−14.6
Exp.^{g}	−16.6	−14.9	−7.6	−16.6

^{a} Shielding tensor at ZORA-BP86/TZ2P. ^{b} Optimized geometry at MP2/SDB-cc-pVTZ. ^{c} Optimized geometry at MP2/ECP+DZP. ^{d} The optimal geometry GED(**2b**) was used as an input geometry with the same model chemistries as for the both computed geometries. ^{e} Shielding tensor at GIAO-MP2/II (IGLO-II basis sets for H, C, B; ECP and DZP for I). ^{f} Data taken from ref. 12a, in which exact assignment on the basis of 2D COSY ^{11}B NMR is missing. ^{g} Data taken from ref. 12d, in which exact assignment using 2D COSY ^{11}B NMR is missing.

The effect of SO coupling on correctly computed ^{11}B NMR chemical shifts can be even more pronounced. For example, in BI$_3$ GIAO computations with the same model chemistry as for **2** cause $\delta(^{11}$B) NMR to be 102.8 ppm whereas the measured value is −7.9 ppm. Inclusion of SO coupling within the ADF scheme improves the fit considerably, *viz* −0.1 ppm. The same trend is observed for BI$_4^-$: GIAO 25.0 ppm, exp. −127.5 ppm, ADF −108.6 ppm.[39] $\delta(^{13}$C) NMR in

halomethyl cations, such as CI_3^+, exhibits the same pattern.[40] However, the pattern of ^{13}C NMR in iodobenzene, a two-dimensional analogue of **2**, is also significantly affected by SO coupling though to a lesser extent than the corresponding chemical shifts in electron deficient boranes and carbocations.[40a] SO contributions for other boron atoms do not exceed 1 ppm, *e.g.* for B(4,5,7,11) in **2** (GED-**2b** geometry) the SO contribution amounts to just 0.05 ppm. B(3,6) even have negative SO contributions. As for the resonances of B(9) and B(12) in **2**, these nuclei exhibit shifts to lower frequencies with respect to **1**, −2.4 ppm, respectively.[9b]

Magnetically-Induced Ring Current Calculations. Aromaticity is a fuzzy concept in chemistry, which can be defined in various ways. Certainly one of the propensities used to describe the aromatic character of a molecule, and one which finds a broad consensus among chemists, is "stabilization due to electron delocalization". In turn, a characteristic of electron-delocalized systems is their strong diamagnetic response in external magnetic fields. This is the basis for the so-called magnetic criterion of aromaticity, implying strong diamagnetism. It is well known that boranes are prime examples of 3-D aromatic systems showing a strong diamagnetic response not only with respect to one relative orientation of the magnetic field (as in the planar Hückel aromatics) but also with respect to any orientation. We have calculated the magnetically-induced current field (DFT-based magnetic response calculations using London orbitals as implemented in the GIMIC program;[28] details see Supporting Information) in $[B_{12}H_{12}]^{2-}$ and found that total induced current (susceptibility) integrates to 18 nA T^{-1}. This can be compared to the case of benzene which displays a total net current of 11 nA T^{-1} (but only when oriented perpendicular to the magnetic field **B**). When magnetic field used to study **2** is set to be perpendicular to a plane containing the carbon and iodine atoms a total current of 15 nA T^{-1} is calculated (see Figure 4); notably, when **B** lies in that plane, a net current of 20 nA T^{-1} results. Thus, the overall diamagnetic response strength of **2** is similar to that for $[B_{12}H_{12}]^{2-}$. However, it shows a distinct anisotropy, giving rise to a smaller diamagnetic response in the plane of the hetero atoms, but remarkably, a larger one

perpendicular to this plane. Using the magnetic criterion we conclude that the overall aromatic character of $[B_{12}H_{12}]^{2-}$ is about equal to that for **2**, though the latter showing clear anisotropy. As was discussed in the NMR section, the chemical shifts of B(9) and B(12) are particularly influenced by relativistic spin-orbit coupling at the iodine atoms *via* the heavy-atom-light-atom (HALA) mechanism.[41] Spin-orbit coupling (SOC) contributes *via* induced spin-density to the current density field.[42] In Figure 5 the SOC contribution to the magnetically-induced current densities in the plane of the carbon and iodine atoms (magnetic field set perpendicular to this plane) is shown. It can be seen that small diatropic (clockwise) current contributions around the atoms B(9) and B(12) are induced *via* SOC, which yields an additional shielding at full-relativistic level of theory of about 22.1 ppm (see Table 2).

Figure 4. Streamline plot of magnetically-induced current density in the plane containing the carbon and iodine atoms for **2**. The magnetic field is set perpendicular to the plot plane. Darker streamlines correspond to stronger currents. The total integrated current susceptibility through a numerically infinite half plane (light blue) amounts to 15 nA T^{-1}.
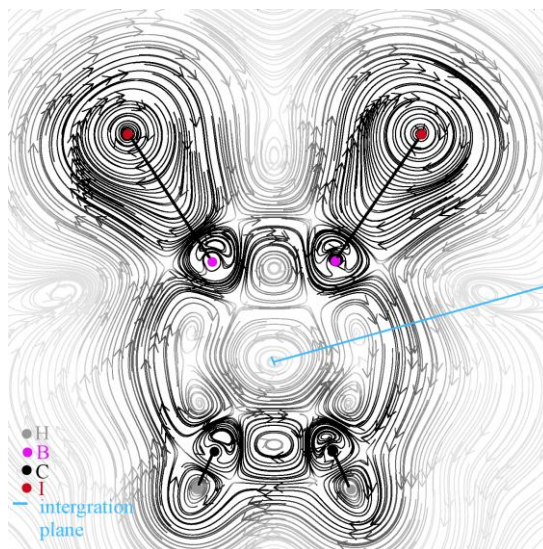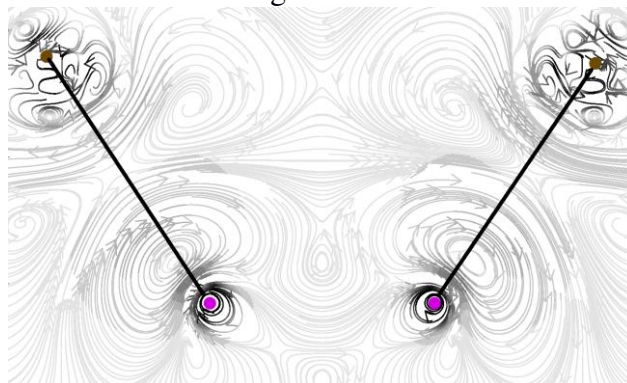
Figure 5. Streamline plot of SOC contribution to the magnetically-induced current density in the plane containing the carbon and iodine atoms for **2**. The magnetic field is set perpendicular to the plot plane. Darker streamlines correspond to stronger currents. The color coding for the elements is the same as in Figure 4.

Further development of the structural chemistry of halogeno derivatives of various heteroboranes, both in the gas-phase and in the crystalline state, is in progress. The study of gas-phase structures can allow the reliability of applied computational protocols to be assessed because of the accurate experimental geometries yielded for heteroboranes with heavier halogens. The complementary study of crystalline structures contributes, as shown recently,[43] to beginning to explain the nature of noncovalent interactions dictating crystal packing forces in crystals.

■ ASSOCIATED CONTENT

Supporting Information

Experimental conditions for the GED experiments for **2** (Table S1), intensities from the GED refinement of **2** (Tables S2 and S3), amplitudes of vibration and distance correction deviations using different methods (Table S4), Z-matrix with initial parameter values used for GED structural refinement for model **2a** (Table S5), Cartesian coordinates description used for optimization in models **2b**-**2e** (Table S6), structural coordinates and amplitudes of vibration and distance corrections from the calculations and GED refinements (Tables S7−S16), correlation matrices for the GED refinements (Tables S17−S21), comparison of geometrical

parameters for models **2c-2e** (Table S22); scattering intensity and background line curves (Figures S1–S5), L-curve (Figure S6), theoretical and experimental radial distribution curves (Figure S7–S10), theoretical and experimental molecular intensity curves (Figures S11–S15). This material is available free of charge via the Internet at http://pubs.acs.org.

■ REFERENCES

1. Olah, G. A.; Prakash, G. K. S.; Williams, R. E.; Field, L. D.; Wade, K. *Hypercarbon Chemistry*; Wiley: New York, 1987.

2. Wade, K. *Electron Deficient Compounds*; Nelson: London, 1971.

3. (a) Burke, A.; Ellis, D.; Giles, B. T.; Hodson, B. E.; Macgregor, S. A.; Rosair, G. M.; Welch, A. J. *Angew. Chem. Int. Ed.* **2003**, *42*, 225; (b) Schleyer, P. v. R.; Najafian, K.; Mebel, A. M. *Inorg. Chem.* **1998**, *37*, 6765.

4. Wiersma, R. J.; Hawthorne, M. F. *Inorg. Chem.* **1973**, *12*, 785.

5. Jemmis, E. D.; Jayasree, E. G.; Parameswaran, P. *Chem. Soc. Rev.* **2006**, *35*, 157.

6.   Hnyk, D.; Všetečka, V.; Drož, L.; Exner, O. *Collect. Czech. Chem. Commun.* **2001**, *66*, 1375.

7.   See, for example, Bühl, M.; Schleyer, P. v. R.; Havlas, Z.; Hnyk, D.; Heřmánek, S. *Inorg. Chem.* **1991**, *30*, 3107.

8.   Hnyk, D.; Rankin, D. W. H. *Dalton Trans.* **2009**, 585 and references therein.

9.   (a) Bohn and Bohn carried out the first GED investigations; see Bohn, R. K.; Bohn, M. D. *Inorg. Chem.* **1971**, *10*, 350; (b) Turner, A. R.; Robertson, H. E.; Borisenko, K. B.; Rankin, D. W. H.; Fox, M. A. *Dalton Trans.* 2005, 1310; (c) Microwave spectroscopy was applied in Samdal, S.; Møllendal, H.; Hnyk, D.; Holub, J. *J. Phys. Chem. A* **2011**, *115*, 3380.

10.   (a) Blake, A. J.; Brain, P. T.; McNab, H.; Miller, J.; Morrison, C. A.; Parsons, S.; Rankin, D. W. H.; Robertson, H. E.; Smart, B. A. *J. Phys. Chem.* **1996**, *100*, 12280; (b) Mitzel, N. W.; Rankin, D. W. H. *Dalton Trans.* 2003, 3650.

11.   Wann, D. A.; Lane, P. D.; Robertson, H. E.; Baše, T.; Hnyk, D. *Dalton Trans.* **2013**, *42*, 12015.

12.   (a) Li, J.; Logan, C. F.; Jones, Jr., M. *Inorg. Chem.* **1991**, *30*, 4866; (b) Zheng, Z.; Jiang, W; Zinn, A. A.; Knobler, C. B.; Hawthorne, M. F. *Inorg. Chem.* **1995**, *34*, 2095; (c) the results of X-ray diffraction analysis are reported in Batsanov, A. S.; Fox, M. A.; Howard, J. A. K.; Hughes, A. K.; Johnson, A. L.; Martindale, S. J. *Acta Cryst. C* **2003**, *59*, 74; (d) Fox, M. A. *PhD Thesis* **1991**, University of Durham, p 102.

13.   Frisch, M. J.; Trucks, G. W.; Schlegel, H. B.; Scuseria, G. E.; Robb, M. A.; Cheeseman, J. R.; Scalmani, G.; Barone, V.; Mennucci, B.; Petersson, G. A.; Nakatsuji, H.; Caricato, M.; Li, X.; Hratchian, H. P.; Izmaylov, A. F.; Bloino, J.; Zheng, G.; Sonnenberg, J. L.; Hada, M.; Ehara, M.; Toyota, K.; Fukuda, R.; Hasegawa, J.; Ishida, M.; Nakajima, T.; Honda, Y.; Kitao, O.; Nakai, H.; Vreven, T.; Montgomery, Jr., J. A.; Peralta, J. E.; Ogliaro, F.; Bearpark, M.; Heyd, J. J.; Brothers, E.; Kudin, K. N.; Staroverov, V. N.;

Kobayashi, R.; Normand, J.; Raghavachari, K.; Rendell, A.; Burant, J. C.; Iyengar, S. S.; Tomasi, J.; Cossi, M.; Rega, N.; Millam, J. M.; Klene, M.; Knox, J. E.; Cross, J. B.; Bakken, V.; Adamo, C.; Jaramillo, J.; Gomperts, R.; Stratmann, R. E.; Yazyev, O.; Austin, A. J.; Cammi, R.; Pomelli, C.; Ochterski, J. W.; Martin, R. L.; Morokuma, K.; Zakrzewski, V. G.; Voth, G. A.; Salvador, P.; Dannenberg, J. J.; Dapprich, S.; Daniels, A. D.; Farkas, Ö.; Foresman, J. B.; Ortiz, J. V.; Cioslowski, J.; Fox, D. J. *Gaussian 09, Revision D.1*, Gaussian, Inc., Wallingford CT, 2009.

14. Frisch, M. J.; Pople, J. A.; Binkley, J. S. *J. Chem. Phys.* **1984**, *80*, 3265.

15. Bergner, M.; Dolg, M.; Küchle, W.; Stoll, H.; Preuss, H. *Mol. Phys.* **1993**, 80, 1431.

16. (a) Sipachev, V. A. *J. Mol. Struct.* (*THEOCHEM*) **1985**, *22*, 143; (b) Sipachev, V. A. *Struct. Chem.* **2000**, *11*, 167; (c) Sipachev, V. A. *J. Mol. Struct.* **2001**, *567*, 67; (d) Sipachev, V. A. *J. Mol. Struct.* **2004**, *693*, 235.

17. Kochikov, I.; Tarasov, Yu.; Kuramshina, G.; Spiridonov, V.; Yagola, A.; Strand, T. *J. Mol. Struct.* **1998**, *445*, 243.

18. Schmidt, M. W.; Baldridge, K. K.; Boatz, J. A.; Elbert, S. T.; Gordon, M. S.; Jensen, J. H.; Koseki, S.; Matsunaga, N.; Nguyen, K. A.; Su, S.; Windus, T. L.; Dupuis, M.; Montgomery, J. A. *J. Comput. Chem.* **1993**, *14*, 1347.

19. Gordon, M. S.; Schmidt, M. W. in *Theory and Applications of Computational Chemistry: The First Forty Years*; Dykstra, C. E.; Frenking, G.; Kim, K. S.; Scuseria, G. E. (Eds); Elsevier: Amsterdam, 2005, pp 1167–1189.

20. (a) Nosé, S. *J. Chem. Phys.* **1984**, *81*, 511; (b) Hoover, W. G. *Phys. Rev. A* **1985**, *31*, 1695.

21. Wann, D. A.; Less, R.; Rataboul, F.; McCaffrey, P. D.; Reilly, A. M.; Robertson, H. E.; Lickiss, P. D.; Rankin, D. W. H. *Organometallics* **2008**, *27*, 4183.

22. Wann, D. A.; Zakharov, A. V.; Reilly, A. M.; McCaffrey, P. D.; Rankin, D. W. H. *J. Phys. Chem. A* **2009**, *113*, 9511.

23. Kutzelnigg, W.; Fleischer, U.; Schindler, M. *The IGLO-Method: Ab Initio Calculation and Interpretation of NMR Chemical Shifts and Magnetic Susceptibilities*; Vol. 23; Springer-Verlag: Heidelberg, 1990.

24. (a) te Velde, G; Bickelhaupt, F. M.; Baerends, E. J.; Fonseca Guerra, C.; van Gisbergen, S. J. A.; Snijders, J. G.; Ziegler, T. *J. Comput. Chem.* **2001**, *22*, 931; (b) Baerends, E. J.; Autschbach, J.; Bérces, A.; Bo, C.; Boerrigter, P. M.; Cavallo, L.; Chong, D. P.; Deng, L.; Dickson, R. M.; Ellis, D. E.; Fan, L.; Fischer, T. H.; Fonseca Guerra, C.; van Gisbergen, S. J. A.; Groeneveld, J. A.; Gritsenko, O. V.; Grüning, M.; Harris, F. E.; van den Hoek, P.; Jacobsen, H.; van Kessel, G.; Kootstra, F.; van Lenthe, E.; McCormack, D. A.; Osinga, V. P.; Patchkovskii, S.; Philipsen, P. H. T; Post, D.; Pye, C. C.; Ravenek, W.; Ros, P.; Schipper, P. R. T.; Schreckenbach, G.; Snijders, J. G.; Sola, M.; Swart, M.; Swerhone, D.; te Velde, G.; Vernooijs, P.; Versluis, L.; Visser, O.; van Wezenbeek, E.; Wiesenekker, G.; Wolff, S. K.; Woo, T. K.; Ziegler, T. *ADF2004.01*, SCM, Theoretical Chemistry, Vrije Universiteit, Amsterdam, The Netherlands..

25. (a) van Lenthe; E.; Baerends, E. J.; Snijders, J. G. *J. Chem. Phys.* **1994**, *101*, 9783; (b) van Lenthe, E.; van Leeuwen, R.; Baerends, E. J.; Snijders, J. G. *Int. J. Quantum Chem.* **1996**, *57*, 281; (c) van Lenthe, E.; Baerends, E. J.; Snijders, J. G. *J. Chem. Phys.* **1993**, *99*, 4597.

26. van Lenthe, E.; Snijders, J. G.; Baerends, E. J. *J. Chem. Phys.* **1996**, *105*, 6505.

27. Onak, T. P.; Landesman, H. L.; Williams, R. E.; Shapiro, I. *J. Phys. Chem.* **1959**, *63*, 1533.

28. a) J. Jusélius, J.; Sundholm, D.; Gauss, J. *J. Chem. Phys.* **2004**, *13*, 3952; b) Fliegl, H.; Taubert, S.; Lehtonen, O.; Sundholm, D. *Phys. Chem. Chem. Phys.* **2011**, *13*, 20500.

29. Berger, R. J. F.; Hoffmann, M.; Hayes, S. A.; Mitzel, N. W. *Z. Naturforsch. B* **2009**, *64*, 1259.

30. Vishnevskiy, Y. V. *J. Mol. Struct.* **2007**, *833*, 30.

31. Vishnevskiy, Y. V. *J. Mol. Struct.* **2007**, *871*, 24.

32. Hargittai, I. *The Gas-Phase Electron Diffraction Technique of Molecular Structure Determination*; in *Stereochemical Applications of Gas-Phase Electron Diffraction; Part A*, Chapter 1, VCH: New York, 1988, pp.1-54.

33. Vishnevskiy, Y. V. *UNEX Version 1.6.0 beta*, http://unexprog.org

34. Hansen, P. C. *Rank-Deficient and Discrete Ill-Posed Problems*; SIAM: Philadelphia, 1998.

35. Fermin, S.; Bazan, V.; Francisco, J. B.; Koung, H. L.; Pelekanos, G. *J. Comput. Appl. Math.* **2012**, *236*, 4264.

36. Ito, K.; Jin, B.; Zou, J. *Applicable Analysis* **2011**, *90*, 1521.

37. Kaupp, M.; Malkina, O. L.; Malkin, V. G.; Pyykkö, P. *Chem. Eur. J.* **1998**, *4*, 118.

38. Kidd, R. G. *Ann. Rep. NMR Spectrosc.* **1980**, *10A*, 2.

39. Hnyk, D.; Macháček, J. XIIth International Congress of Quantum Chemistry, Kyoto, Japan, May 21-26, C176, 2006.

40. a) Kaupp, M.; Malkina, O. L.; Malkin, V. G. *Chem. Phys. Lett.* **1997**, *265*, 55; b) Krossing, I.; Bihlmeier, A.; Raabe, I.; Trapp, N. *Angew. Chem. Int. Ed.* **2003**, *42*, 1531.

41. Kaupp, M.; Malkina, O. L.; Malkin, V. G.; Pyykkö, P. *Chem. Eur. J.* **1998**, *4*, 118.

42. Berger, R. J. F.; Repisky, M.; Komorovsky, S. *Chem. Commun.* **2015**, *51*, 13961.

43. Fanfrlík, J.; Přáda, A.; Padělková, Z.; Pecina, A.; Macháček, J.; Lepšík, M.; Holub, J.; Růžička, A.; Hnyk, D.; Hobza, P. *Angew. Chem. Int. Ed.* **2014**, *53*, 10139.

■ **TOC graphic and synopsis**

Two iodine atoms antipodally coupled with two carbons of the C_{2v}-symmetrical icosahedral carbaborane produce a negligible effect on the cage geometry in the gas phase. Their response to the external magnetic field is dominated by spin-orbit coupling with boron atoms to which they are bonded.